PCCP

PAPER

Cite this: *Phys. Chem. Chem. Phys.*, 2016, **18**, 2535

An experimental and theoretical study of core–valence double ionisation of acetaldehyde (ethanal)

S. Zagorodskikh,[ab] M. Vapa,[cd] O. Vahtras,[c] V. Zhaunerchyk,[ab] M. Mucke,[a] J. H. D. Eland,[abe] R. J. Squibb,[ab] P. Linusson,[f] K. Jänkälä,[g] H. Ågren[c] and R. Feifel*[ab]

Received 25th September 2015,
Accepted 23rd November 2015

DOI: 10.1039/c5cp05758b

www.rsc.org/pccp

Core–valence double ionisation spectra of acetaldehyde (ethanal) are presented at photon energies above the carbon and oxygen 1s ionisation edges, measured by a versatile multi-electron coincidence spectroscopy technique. We use this molecule as a testbed for analyzing core–valence spectra by means of quantum chemical calculations of transition energies. These theoretical approaches range from two simple models, one based on orbital energies corrected by core valence interaction and one based on the equivalent core approximation, to a systematic series of quantum chemical electronic structure methods of increasing sophistication. The two simple models are found to provide a fast orbital interpretation of the spectra, in particular in the low energy parts, while the coverage of the full spectrum is best fulfilled by correlated models. CASPT2 is the most sophisticated model applied, but considering precision as well as computational costs, the single and double excitation configuration interaction model seems to provide the best option to analyze core–valence double hole spectra.

I. Introduction

The absorption of a single, comparatively high energy photon may result in not only a single valence or core electron being removed, as widely studied by conventional electron spectroscopy methods, but also several electrons being ejected. The removal of several electrons can occur either simultaneously or step-wise and either from the same shell or from different shells, and can be regarded as a manifestation of electron correlation leading to the formation of electronic states of multiply-ionised systems which are often only little explored.

The time-of-flight photoelectron–photoelectron coincidence (TOF-PEPECO) spectroscopy technique introduced by Eland *et al.*[1] provides an efficient way to study the electronic states associated with the ejection of several electrons at sufficient resolution for kinetic energies up to a few hundred eVs. To begin with, this technique utilized a pulsed helium lamp which allowed the investigation of double ionisation processes involving valence shells (see *e.g.* ref. 1–6). In order to study double and higher order ionisation processes involving inner shells, more energetic photons are needed as provided by synchrotron radiation sources. An example of such processes, which the present study focusses on, is core–valence double ionisation where a valence and an inner shell electron are removed upon photon absorption. This process was investigated in the past for rare gas atoms such as neon[7] and krypton[8] as well as for small molecular systems such as N_2,[7] CO,[9] O_2,[10] CS_2,[11] OCS[12] and SO_2.[13] In several of those studies, the core–valence states have been assigned using different quantum chemical computational techniques (*e.g.* "independent particle" open-shell Hartree–Fock method, multi-configuration self-consistent field (MCSCF) method, restricted active space method, and density functional theory (DFT)). In some of the previous works[10,11] a one-to-one correspondence of the core–valence photoionisation spectra to their associated conventional valence band photoelectron spectra was noticed which led to a very simple explanation of the observed core–valence spectra. These interpretations were also supported by quantum chemical calculations.

Acetaldehyde is an organic compound chemically denoted as CH_3CHO. It contains two carbon atoms in different chemical environments which makes it interesting for further investigations of single-photon core–valence double ionisation. It belongs

[a] *Department of Physics and Astronomy, Uppsala University, Box 516, SE-751 20 Uppsala, Sweden*
[b] *Department of Physics, University of Gothenburg, Origovägen 6B, SE-412 96 Gothenburg, Sweden. E-mail: raimund.feifel@physics.gu.se*
[c] *Department of Theoretical Chemistry and Biology, School of Biotechnology, KTH Royal Institute of Technology, SE-106 91 Stockholm, Sweden*
[d] *Centre for Molecular Materials Research, University of Oulu, P.O. Box 3000, 90014 Oulu, Finland*
[e] *Department of Chemistry, Physical and Theoretical Chemistry Laboratory, Oxford University, South Parks Road, Oxford OX1 3QZ, UK*
[f] *Department of Physics, Stockholm University, AlbaNova University Center, SE-106 91 Stockholm, Sweden*
[g] *Department of Physics, University of Oulu, 90014 Oulu, Finland*

to the C_s symmetry group, and within this symmetry group its neutral ground state configuration can be denoted as:

$$\text{core } (4a')^2(5a')^2(6a')^2(7a')^2(1a'')^2(8a')^2(9a')^2(2a'')^2(10a')^2$$

where the core part comprises the atomic-like[14] O1s, $C_1$1s, $C_2$1s orbitals, which will be denoted as such in what follows. Of the two chemically different carbon atoms, the first one refers to the formylic and the second one to the methylic group, respectively. The remaining orbitals are considered to be essentially of valence character (denoted in what follows as v). Also, the a′ orbitals will sometimes be referred to as σ orbitals and the a″ as π orbitals.

The electronic structure of the acetaldehyde molecule was investigated in the past by different techniques, in particular single-channel experimental techniques such as ultraviolet photoelectron spectroscopy (UPS),[15–20] X-ray photoelectron spectroscopy (XPS),[20,21] and Auger electron spectroscopy.[21,22] Whereas UPS and XPS have provided detailed information on the electronic states of the cation, Auger electron spectroscopy has revealed information on the dicationic states associated with double valence vacancies. Very recently, a complementary study of the dicationic valence states of acetaldehyde has been performed[23] with the present time-of-flight multi-electron coincidence technique.

The relative simplicity of the acetaldehyde molecule makes it a good test case where resolved experimental core–valence double hole structures can be analyzed by systematically refined theoretical models. In order to assign the spectral features observed we scrutinize the previously established empirical model using normal valence spectra.[10,11] We then launch two models, of which one is based on interaction corrected "Koopmans theorem" orbital energies and on the second one on the equivalent core approximation, and complement these with the application of a systematic series of quantum chemical methods of higher sophistication.

II. Experimental and analysis details

For the experiments we utilized a versatile multi-electron coincidence spectroscopy technique based on a magnetic bottle,[1] which reveals efficiently the electronic states of multiply ionised systems and gives crucial information on the formation of such states and the energy sharing of the emitted electrons. Briefly, essentially all the electrons emitted by the target sample into the solid angle of 4π are confined by a combination of a strong and weak magnetic field[24] and are guided to an about 2 m distant multi-channel plate detector with multi-hit capability.

The experiments were carried out at beam line U49/2 PGM-1 of the synchrotron radiation facility BESSY-II at the Helmholtz Zentrum in Berlin which covers the photon energy range of 85 eV up to about 1600 eV. We recorded multiple coincidence events of electrons emitted by acetaldehyde at the photon energies of 350 eV and 600 eV. The energy resolution of the monochromator was set to about 300 meV or better. The storage ring was operated in single bunch mode, providing 30 ps long light pulses at a repetition rate of about 1.25 MHz. In order to further reduce the rate of the radiation pulses for unambiguous time referencing of our experiment, we used a mechanical chopper,[25] synchronized to the radio frequency signal of the storage ring.

A commercially available sample of acetaldehyde with a stated purity >99% was used for the experiments. The vapor pressure of acetaldehyde at room temperature was sufficiently high for achieving a sample gas density in the interaction region of the spectrometer suitable for the experiments without additional heating. In order to remove impurities due to air exposure, when connecting the sample holder to our spectrometer set-up, we used several freeze–pump–thaw cycles. The purity of the sample was verified by recording conventional electron spectra both in the valence and core regions in comparison with their spectra known from the literature.[15–17,19,20]

The flight time to kinetic energy conversion is based on

$$E_{\text{kin}} = \frac{D^2}{(t - t_0)^2} + E_0 \quad (1)$$

where t denotes the measured flight time, E_{kin} the electron kinetic energy, and where D (which contains the length of the flight path), t_0 and E_0 are calibration parameters derived by least-square fitting of the spectral features to reference spectra. For the calibration of the kinetic energy scale, we used the Argon L_2 and L_3 photoelectron lines[26] recorded for several photon energies as well as the core ionisation energies of acetaldehyde well known from the literature.[21]

Because the main decay path of core vacancies of light atoms such as carbon and oxygen is Auger decay, the core–valence double ionisation data were extracted from triple coincidence events, where the first arrival electron is a fast Auger electron, which is expected to be in the range of 220–270 eV for the decay of states involving carbon 1s vacancies and about 510–570 eV for the decay of the states involving the oxygen 1s hole.[21,23] The flight times of the two remaining electrons are then represented in the form of a two-dimensional coincidence map, using a bin size of 100 ps, which corresponds to the chosen time resolution of the time-to-digital converter used in the experiment.

In converting the data from the flight time to the energy domain, the dependence of the bin size in the energy domain needs to be taken into account adequately, because of the non-linearity of the conversion formula (*cf.* eqn (1)); *i.e.* the constant time bin is converted to a smaller energy bin size for the slow flight time end of the spectra and a larger size for the fast flight time end, which affects the intensity information. This has been taken into account for the different figures in the present work by defining a grid in the energy domain with a fixed bin size in the range of 50–200 meV, and redistributing the intensity based on the degree of overlap between the bins of the time and energy grids. The core–valence ionisation process is expected to constitute a series of diagonal lines on the coincidence map (*cf.* Fig. 1 and 2) which each represent a value of the excess energy (*i.e.* the sum of two kinetic energies) arbitrarily shared by the two electrons. To obtain the core–valence electron spectra, the intensity along the diagonal lines is summed.

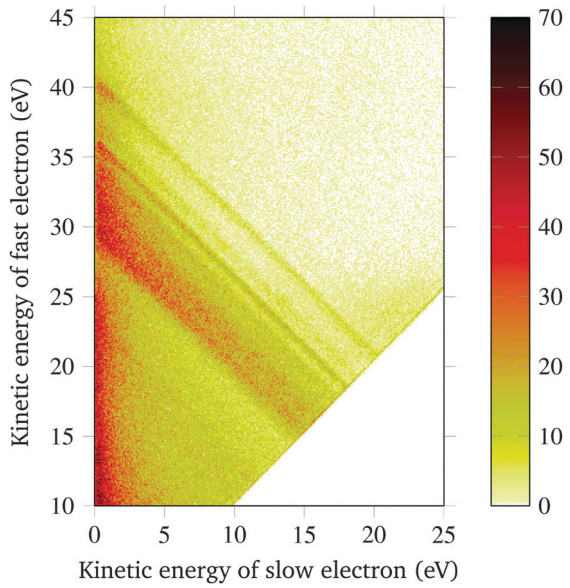

Fig. 1 Coincidence map of acetaldehyde formed by electron pairs detected in coincidence with thirdly emitted carbon Auger electrons. The data were obtained at the photon energy of 350 eV. The straight diagonal lines reflect the formation of $C1s^{-1}v^{-1}$ states. The bin size is 100 meV.

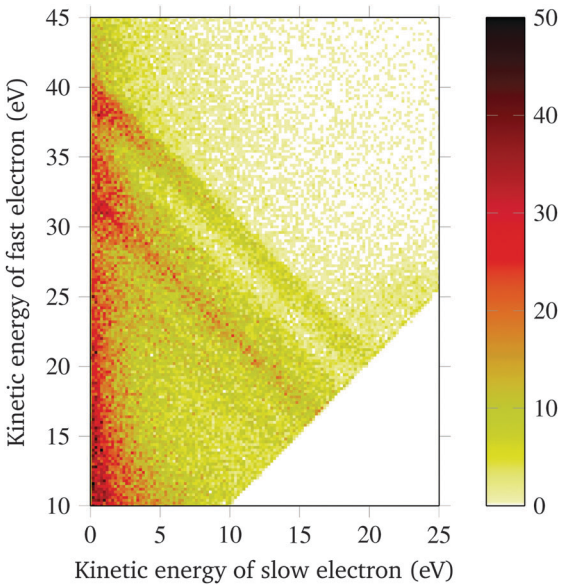

Fig. 2 Coincidence map of acetaldehyde formed by electron pairs detected in coincidence with thirdly emitted oxygen Auger electrons. The data were obtained at the photon energy of 600 eV. The straight diagonal lines reflect the formation of $O1s^{-1}v^{-1}$ states. The bin size is 200 meV.

III. Theoretical details

From a theoretical point of view core–valence states pose a particular challenge. On one hand they call for a self-consistent field (SCF) procedure to deal with substantial relaxation energies and orbital transformations associated with the creation of a core hole. On the other hand, valence ionisation is best treated with perturbational or Green's function approaches as the difference in electron correlation between the ground state and a valence ionised state is relatively small, at least for outer valence states, and is associated with relatively small orbital relaxation. Furthermore, optimizing orbitals for the valence hole state may not improve the energetics because in many cases (and models) the ''relaxation'' and ''correlation'' energies counteract, which also often is the ground for the relative success of Koopmans' theorem.

While there is abundant work for valence ionisation spectra that has addressed these issues, the available literature on core–valence modeling is scarce. Calculations of core–valence spectra of molecular oxygen were carried out in the work by Andersson *et al.*,[8,10,11] and further refined by Niskanen *et al.* for the cases of the OCS[12] and CS_2[13] molecules. These studies utilized a SCF procedure to optimize the individual two-hole states, where each wave function was expanded in configurations – thus using MCSCF approaches. They applied so-called restricted active spaces where the orbital of the ionised core was restricted to be singly occupied. More specifically, a first orbital space was used to accommodate the singly occupied core orbital, a second space was used for complete electron distributions among valence orbitals, and a third space was optionally used for the excitation of a small number of electrons to empty orbitals. The selection and division of the active spaces can be guided by the occupation numbers from Møller–Plesset perturbation theory.[27] This is also the approach we initially take in the present investigation. By enforcing single occupancy we hinder collapse of the wave function to a valence doubly ionised state, which else would be the consequence of the variational procedure. Moreover, an initial restriction is applied to the set of orbitals in the sense that a two-step, second-order optimization procedure for the core–valence states is applied to avoid orbital collapse. Here an intermediate optimization step with the core orbital frozen brings the wave function to the local region, followed by a full variational step using a Newton–Raphson technique relaxing also the core orbital. This procedure provides full optimization of highly excited core states, and as shown by Niskanen *et al.*[13] this holds also for core–valence states.

In the work on CS_2 by Andersson *et al.*[11] this procedure was shown to work well for core–valence ionisation also for symmetry adapted core orbitals, and that both symmetry restricted and symmetry broken solutions could be obtained within the scheme. In the paper on OCS by Niskanen *et al.*[12] further corrections were analyzed. One is the dynamical correlation which is left out from a complete active space (without the third correlating space) that is designed to preferentially cope with valence, near-degenerate, electronic excitations. A correction was included by assuming N-electron valence space perturbation theory of second order (NEVPT2) as applied for the ground state and the core–valence doubly ionised states. Here the perturbative correction of the core–valence state (the lowest of a symmetry) was modeled by using the $Z + 1$ approximation to the core-hole site, which mimicks the resonance valence electronic structure for the core–valence hole state in question. By applying the $Z + 1$ approximation, which thus replaces a core hole by an additional nuclear charge, to the corresponding

complete-active-space (CAS) an estimate of the perturbational (dynamic correlation) contribution to the double ionisation energies was obtained.

The present work acknowledges the investigations mentioned and takes a further step in analyzing also excited core–valence states. We assume a combined MCSCF – CI (configuration interaction) procedure. Full MCSCF has the potential disadvantage of optimizing several multi-electron excited states with low energy but without sizable transition moment before a state with intensity is obtained. If the states are not orthogonalized (or non-state-interactive) further hindrance in the interpretation is imposed. In the present work this is even more compelling as the formation of core–valence states is not clearly defined by selection rules. We therefore believe a better approach for the excited states is configuration interaction based on a fixed set (or fixed sets) of orbitals, a technique long tested in quantum chemistry.[28] In this way a sizable portion of the core–valence energy spectrum is spanned and at a much smaller computational cost than state-by-state MCSCF.

As an additional simple way to analyze the spectra, to the best of our knowledge not tried before, is to apply a Koopmans' theorem type approach to the equivalent core species for obtaining the energy spectrum of core–valence states with the core ionisation potential (IP) as reference. We note that Koopmans' theorem will not hold strictly in such a case, since the core–valence exchange interaction is not properly treated by the $Z + 1$ approximation. Thus if the core hole species are replaced by $Z + 1$ species (here O by F, and C by N) and optimized by Hartree–Fock of the corresponding cationic species, the negative of the canonical orbital energies gives an estimate of the spectrum.

The Koopmans' theorem in its classical form gives the eigenvalues of the Fock matrix a physical interpretation, as the ionisation potential in a frozen-orbital approximation. With $E[\mathrm{gs}]$ being the ground state (gs) energy of a given Hamiltonian H,

$$E[\mathrm{gs}] = \langle \mathrm{gs}|H|\mathrm{gs}\rangle \tag{2}$$

and applying the rules for evaluating matrix elements involving Slater determinants, the energy of a singly ionised state $E[\mathrm{v}^{-1}]$, corresponding to the removal of an electron in orbital ϕ_v, is

$$E[\mathrm{v}^{-1}] = \langle \mathrm{v}^{-1}|H|\mathrm{v}^{-1}\rangle = E[\mathrm{gs}] - F_\mathrm{vv} \tag{3}$$

where the closed-shell Fock matrix F is a combination of one-electron (h_pq) and two-electron integrals (pq|rs):

$$F_\mathrm{pq} = h_\mathrm{pq} + \sum_k^{\mathrm{occ}} 2(\mathrm{pq}|kk) - (\mathrm{p}k|k\mathrm{q}). \tag{4}$$

$$h_\mathrm{pq} = \int \mathrm{d}V \phi_\mathrm{p}(\vec{r}) \left(-\frac{\nabla^2}{2} + \sum_N \frac{Z_N}{|\vec{r} - \vec{R}_N|} \right) \phi_\mathrm{q}(\vec{r}) \tag{5}$$

$$(\mathrm{pq}|\mathrm{rs}) = \iint \mathrm{d}V_1 \mathrm{d}V_2 \frac{\phi_\mathrm{p}(\vec{r}_1)\phi_\mathrm{q}(\vec{r}_1)\phi_\mathrm{r}(\vec{r}_2)\phi_\mathrm{s}(\vec{r}_2)}{|\vec{r}_1 - \vec{r}_2|} \tag{6}$$

h_pq thus consists of the kinetic energy of a given electron and the electrostatic interaction energy with nuclei located at sites $\vec{R}_N$ with charge Z_N. All indices refer to molecular orbitals ϕ and the summation in eqn (4) is over the subset of doubly occupied orbitals (k) in the ground state. With so-called canonical Hartree–Fock orbitals, this matrix is diagonal with eigenvalues ε_p, and Koopmans' theorem gives that the ionization potential, the energy difference ΔE between the ionized and ground states, is

$$\Delta E = E[\mathrm{v}^{-1}] - E[\mathrm{gs}] = -\varepsilon_\mathrm{v}. \tag{7}$$

A similar approach to two-electron core–valence removal can be derived. With α,β as the spin-projection $\left(\pm\frac{1}{2}\right)$ of a given electron, the energy of the final singlet (+) and triplet (−) states is given by

$$\begin{aligned} &= \left\langle \frac{\mathrm{c}_\alpha{}^{-1}\mathrm{v}_\beta{}^{-1} \pm \mathrm{c}_\beta{}^{-1}\mathrm{v}_\alpha{}^{-1}}{\sqrt{2}} | H | \frac{\mathrm{c}_\alpha{}^{-1}\mathrm{v}_\beta{}^{-1} \pm \mathrm{c}_\beta{}^{-1}\mathrm{v}_\alpha{}^{-1}}{\sqrt{2}} \right\rangle \\ &= \left\langle \mathrm{c}_\alpha{}^{-1}\mathrm{v}_\beta{}^{-1}|H|\mathrm{c}_\alpha{}^{-1}\mathrm{v}_\beta{}^{-1}\right\rangle \pm \left\langle \mathrm{c}_\alpha{}^{-1}\mathrm{v}_\beta{}^{-1}|H|\mathrm{c}_\beta{}^{-1}\mathrm{v}_\alpha{}^{-1}\right\rangle. \end{aligned} \tag{8}$$

A closed-shell ground state is assumed in the last step which allows for a reduction in number of terms. The first of these terms can be expanded to

$$\left\langle \mathrm{c}_\alpha{}^{-1}\mathrm{v}_\beta{}^{-1}|H|\mathrm{c}_\alpha{}^{-1}\mathrm{v}_\beta{}^{-1}\right\rangle = \langle H\rangle - \varepsilon_\mathrm{c} - \varepsilon_\mathrm{v} + J_\mathrm{cv} \tag{9}$$

i.e. the sum of the individual ionisation energies and the Coulomb repulsion integral between the core and valence electrons $J_\mathrm{cv} = (\mathrm{cc}|\mathrm{vv})$. The presence of this term explains why a shifted valence spectrum with a fixed amount may coincide with the measured core–valence spectrum (see below Fig. 1 and 2) for some peaks but not for others, as the repulsion between individual core–valence pairs may vary substantially.

The second term in eqn (8) reduces to the exchange integral which accounts for the singlet–triplet splitting

$$\left\langle \mathrm{c}_\alpha{}^{-1}\mathrm{v}_\beta{}^{-1}|H|\mathrm{c}_\beta{}^{-1}\mathrm{v}_\alpha{}^{-1}\right\rangle = (\mathrm{cv}|\mathrm{vc}) \equiv K_\mathrm{cv}. \tag{10}$$

The equivalent of Koopmans' theorem for two-electron removal is then

$$\Delta E = -\varepsilon_\mathrm{c} - \varepsilon_\mathrm{v} + J_\mathrm{cv} \pm K_\mathrm{cv}. \tag{11}$$

It should be remembered that this relation only gives a qualitative interpretation of the spectrum. Electrons which are close in space will have larger electron repulsion (J values) and will show an increased binding energy as a pair, compared to the sum of the respective ionisation potentials. Electrons that are localized in regions that are far apart will have small repulsion energies and pair ionisation energies will be close to the sum of the individual ionisation potentials. However when core electrons are involved, the qualitative results of this approximation are of limited value as one neglects large orbital relaxation effects and associated rearrangement of charge.

The $Z + 1$ approximation for the doubly ionised states aims for a simple description which includes the most important relaxation effects, and represents an equivalent-core approximation for the valence electrons. Using the open-shell core-hole state as reference level there is not a single Fock matrix that allows for an interpretation like Koopmans' theorem, but there are two (they can be represented in different ways, the most

common being α- and β-Fock matrices). However, for a given choice of molecular orbitals we can always show that

$$\langle c_\alpha^{-1} v_\beta^{-1} | H | c_\alpha^{-1} v_\beta^{-1} \rangle = E[c_\alpha^{-1}] - F_{vv}^{\beta} \quad (12)$$

where the β-Fock matrix for a core-hole reference state with the open shell in an α state, is

$$F_{pq}^{\beta} = h_{pq} + (pq|cc) + \sum_{k \neq c}^{occ} 2(pq|kk) - \sum_{k}^{occ} (pk|kq). \quad (13)$$

The $Z + 1$ approximation can now be understood from a rearrangement of the terms

$$F_{pq}^{\beta} = \left[h_{pq} - (pq|cc)\right] + \sum_{k}^{occ} 2(pq|kk) - (pk|kq) \quad (14)$$

i.e. to a closed-shell Fock matrix expression with a corrected one-electron term. We now make the approximation

$$h_{pq}(Z) - (pq|cc) \approx h_{pq}(Z + 1) \quad (15)$$

where Z refers to the nuclear charge of the atom where the core orbital is centered. This is exact in the limit when the core-hole orbital approaches a delta function on the equivalent nucleus. The result is that we have an equivalent closed-shell system with an increased nuclear charge and

$$\Delta E[c^{-1}v^{-1}] \approx E[c^{-1}] - \varepsilon_v \pm K_{cv}. \quad (16)$$

An approximate valence ionisation energy for the core-hole system can thus completely be calculated from the equivalent-core system, its orbital energies and exchange integrals. In the calculations presented here, we use the relaxed total core-hole energy in eqn (16).

As spin or spin projection is not discriminated in the measurements, we assume, as in the previous work of Niskanen *et al.*,[13] that both spin singlet and triplet states are represented. Their separation for a given core–valence double ionisation process gives a measure of the overlap and exchange of the two, core and valence, orbitals. With all possible spin projections present for the two continuum electrons we assume that the residual states appearing in the spectra observed are statistically populated, thus 3/1 for triplets to singlets ratio. We may speculate that the final states are created in a sudden fashion, with the two continuum orbitals strongly orthogonal to the residual state wave functions. This would lead to ''shake'' structures and a modulation of the intensities by the squared overlap amplitudes. These in turn are, in analogy to ordinary core level spectra, roughly guided by the squares of the CI coefficients for the main configuration. The total intensities are also guided by transition moments to the continuum, which for ionisation may be strongly varying with energy closer to threshold.

IV. Results and discussions

Fig. 1 and 2 display coincidence maps of two electrons extracted upon core–valence double ionisation of acetaldehyde at the photon energies of 350 eV and at 600 eV, respectively. The latter was recorded above the oxygen 1s core ionisation threshold (538.64 eV[21]) and the former above the two chemically different carbon 1s core ionisation thresholds, *i.e.* formylic (294.45 eV[21]) and methylic (291.8 eV[21]), respectively. Because upon single photon absorption the valence and the core electrons are removed simultaneously, the two emitted electrons share the excess energy arbitrarily. This makes it impossible to distinguish in the data extraction the origin of the two electrons involved in the double ionisation step. This implies in particular in the case of carbon 1s – valence double ionisation that, from an experimental point of view, we cannot extract pure (or ''site-specific'') formylic or methylic carbon core–valence spectra of acetaldehyde. The background electrons evenly distributed in the time scale, produce more intensity in the low energy region due to the non-linearity of the conversion, in particular, the fact, that for the signal attributed to slower electrons, one energy bin corresponds to more time bins, but as one can see from the maps, this effect has a minor impact on the core–valence ionisation anti-diagonal lines.

Fig. 3 and 4 present core–valence double ionisation spectra (dotted curves) of acetaldehyde obtained from the coincidence maps in the way described above in the Section 2. Those spectra reflect $C1s^{-1}v^{-1}$ and $O1s^{-1}v^{-1}$ states, respectively.

A. Core–valence double ionisation involving carbon 1s vacancies ($C1s^{-1}v^{-1}$)

The core–valence double ionisation spectrum of acetaldehyde involving carbon 1s vacancies, displayed in Fig. 3, reflects in the low energy part several comparatively sharp features. Their energetic location is given in the left panel of Table 1. We reckon that the relative energy spacing of the first two core–valence structures is very similar to the energy spacing of the two lowest features in the known valence photoelectron spectrum of acetaldehyde.[15–17,19,20] This motivates us to compare the core–valence spectrum directly to the valence band photoelectron spectrum of *e.g.* Keane *et al.*[20] by shifting the latter such that it lines up with the lowest core–valence features 1 and 2, and by convoluting it with a Gaussian of 0.7 eV full width at half maximum (FWHM), as shown in the lower panel of Fig. 3. The FWHM value takes into account the present experimental resolution and is chosen to provide a very good agreement with peak structure 1. Although, a fairly good agreement can be obtained for the two lowest features, structures 3 and onwards cannot so easily be explained. Since acetaldehyde consists of two chemically different carbon atoms, peak 3 might be associated with a core–valence state which involves primarily the somewhat deeper lying formylic 1s hole. Therefore, we also shifted the valence photoelectron spectrum such that its lowest structure lines up with peak 3, as shown in the upper panel of Fig. 3. As can be seen, again, the structures higher up in ionisation energy cannot be so easily explained in this way.

Also, a superposition of two adequately shifted valence band photoelectron spectra, even when their relative intensities are weightened according to the relative intensity ratio of the two peak structures 1 and 3 (instead of using equal weights because of similar C1s ionisation cross sections expected) does not

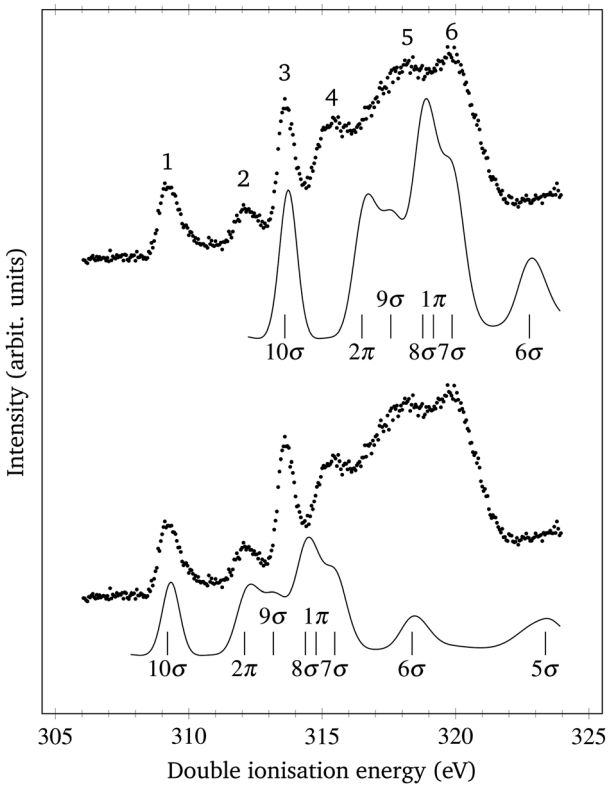

Fig. 3 Experimental core–valence double ionisation spectrum of acetaldehyde reflecting the formation of $C1s^{-1}v^{-1}$ states recorded at the photon energy of 350 eV, shown as dots. The single valence photoelectron spectrum measured by Keane *et al.*,[20] convoluted with a Gaussian function of 0.7 eV width (FWHM) and shifted by 298.97 eV (lower panel) and 303.37 eV (upper panel), respectively, is included for direct comparison. The bin size is 50 meV.

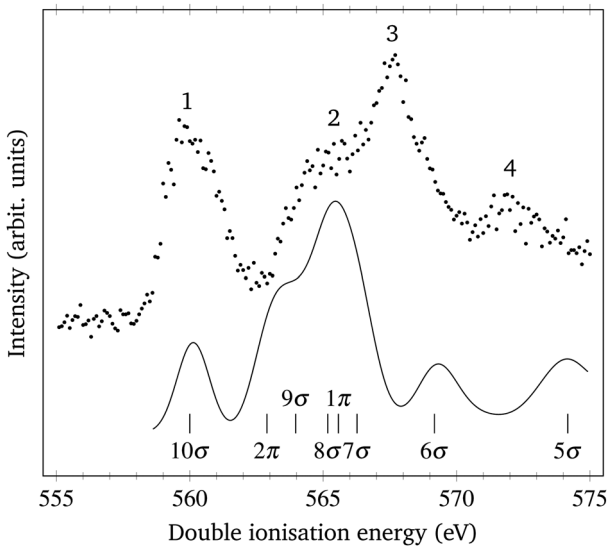

Fig. 4 Experimental core–valence double photoionisation spectrum of acetaldehyde reflecting the formation of $O1s^{-1}v^{-1}$ states recorded at the photon energy of 600 eV, shown as dots. The single valence photoelectron spectrum measured by Keane *et al.*,[20] convoluted with a Gaussian function of 1.4 eV width (FWHM) and shifted by 549.77 eV is included for direct comparison. The bin size is 100 meV.

Table 1 Energy positions (center values where possible) of spectral features of the experimental core–valence spectra. The left part gives double ionisation energies for features from the spectrum recorded above the C 1s ionisation thresholds, following the numbering of Fig. 3. The right part gives accordingly double ionisation energies for features from the spectrum recorded above the O 1s threshold, following the numbering of Fig. 4

$C1s^{-1}v^{-1}$		$O1s^{-1}v^{-1}$	
Number	Ionization energy	Number	Ionization energy
1	309.2	1	560.2
2	312.1	2	565.5
3	313.6	3	567.5
4	315.6	4	571.9
5	318.1		
6	319.7		

result in a better agreement with the experimental core–valence spectrum. This may suggest that some higher methylic core–valence states also contribute to peak 3.

B. Core–valence photoionisation involving oxygen 1s vacancy ($O1s^{-1}v^{-1}$)

Fig. 4 shows the oxygen core–valence spectrum of acetaldehyde which essentially consists of four distinct features: a first peak 1 at about 560.2 eV ionisation energy followed by a double peak structure with an onset at about 563.1 eV, a first local maximum 2 at 565.5 eV and a relatively sharp maximum 3 at about 567.5 eV, as well as a somewhat weaker peak structure 4 at 571.9 eV ionisation energy. We note that the overall form of the spectrum is reminiscent to previously published core–valence spectra involving an O1s vacancy, in particular for the cases of O_2[10] and OCS.[12] In the case of SO_2[13] the O1s-valence spectrum reflects a double peak structure in the lower ionisation energy part, and is, apart from that, also quite similar in structure to the spectrum presented here.

In order to get a first idea on a possible interpretation of this core–valence spectrum of acetaldehyde, we shifted the single valence photoelectron spectrum by 549.77 eV to line up with the lowest feature of the core–valence spectrum, and broadened it by a Gaussian function of 1.4 eV FWHM, which is twice the width compared to the carbon case. We attribute this change in width primarily to the reduced experimental resolution at higher photon energies, while the shorter lifetime of the oxygen 1s hole in comparison to the lifetime of the carbon C1s vacancy is, in principle, also a factor.

As can be seen, whereas the lowest feature might be understood in terms of the involvement of the 10σ valence orbital, the agreement for the higher states is again not very good. In shifting the valence photoelectron spectrum about 2 eV higher up, one can obtain visually a somewhat better agreement for features 2, 3 and 4, but then the structure at the lowest core–valence ionisation energy remains unexplained.

C. Numerical results in comparison to experimental results

In order to better understand the core–valence spectra of acetaldehyde, we analyzed the experimental data presented in

Fig. 3 and 4 by means of a series of quantum chemical calculations outlined in Section 3. The numerical results obtained are graphically displayed in Fig. 5–14 together with the experimental spectra for direct comparison. Tables 2–5 summarize the numerical results of this study at various levels of theory, and are ordered according to their level of sophistication. At all levels of theory the six highest roots in the A' symmetry and two roots in the A'' symmetry have been calculated. The theoretical results are sorted as follows: in Table 4 we present the single-determinant models and in the Table 5 the correlated models. This means in particular, in Table 4 the results of the Koopmans', the $Z + 1$ approximation, and Hartree–Fock calculations are given. Each final state is uniquely characterized by the core–valence pair and is labeled accordingly. In Table 5, the results of CAS, SDCI (single-double configuration interaction), and CASPT2 calculations are given and the states are simply ordered by core, symmetry and energy.

At the Koopmans' level we lack the relaxation energy which is known to be substantial for the core-hole state alone. The calculated values are based on the orbital energies and integrals of Table 2. Generally speaking, these results are only useful given an appropriate shift of the whole spectrum, *e.g.* by the core-hole relaxation energy, but in Table 4 we provide the results as calculated.

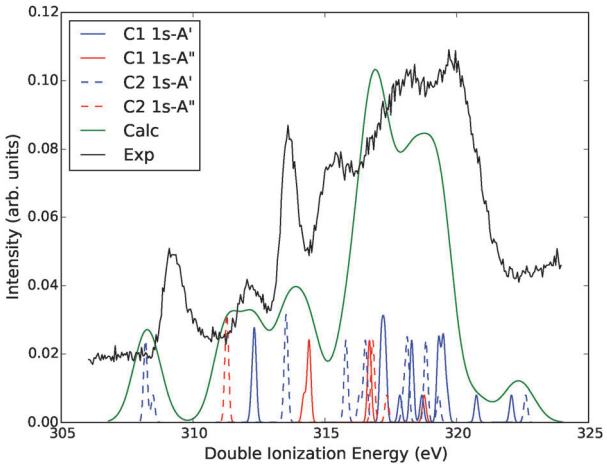

Fig. 7 MCSCF results of $C1s^{-1}v^{1}$.

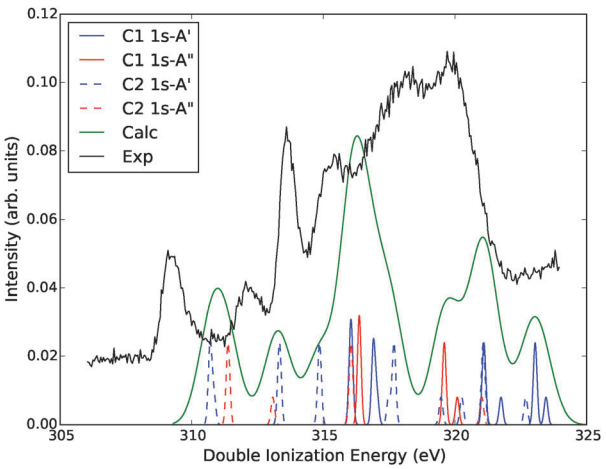

Fig. 5 Results of the $Z + 1$ approximation for $C1s^{-1}v^{1}$.

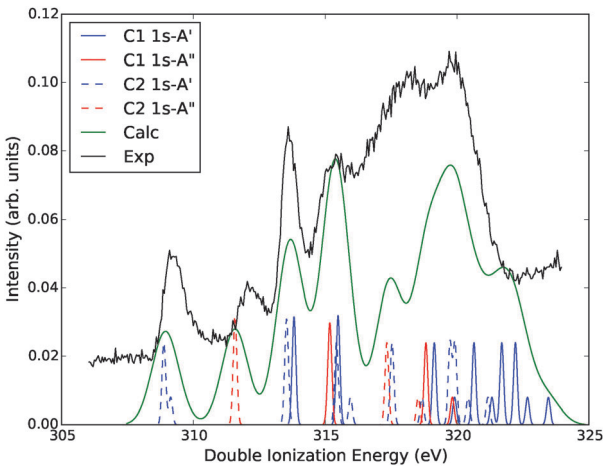

Fig. 8 SDCI results of $C1s^{-1}v^{1}$.

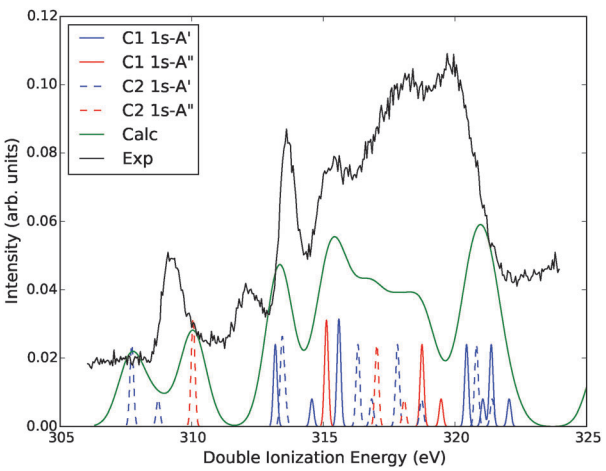

Fig. 6 Hartree–Fock results of $C1s^{-1}v^{1}$.

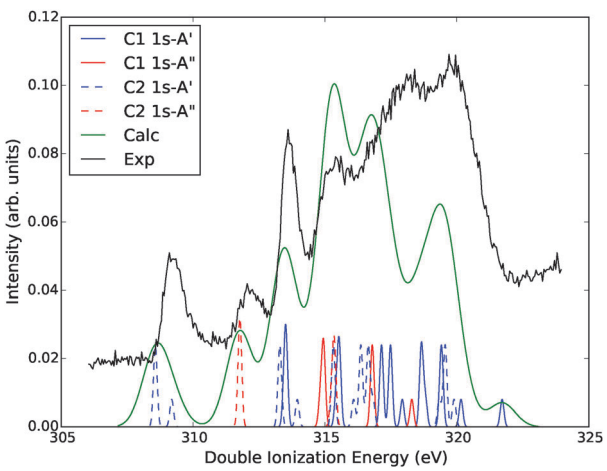

Fig. 9 CASPT2 results of $C1s^{-1}v^{1}$.

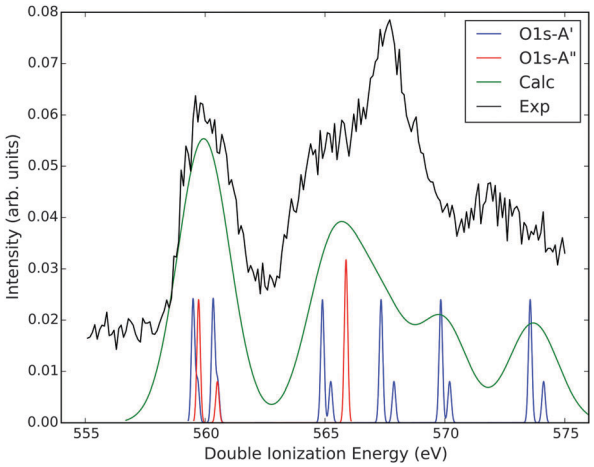

Fig. 10 Results of the $Z + 1$ approximation for $O1s^{-1}v^{1}$.

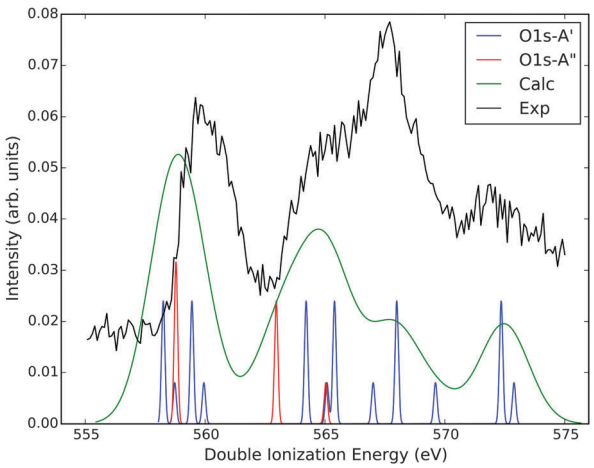

Fig. 11 Hartree–Fock results of $O1s^{-1}v^{1}$.

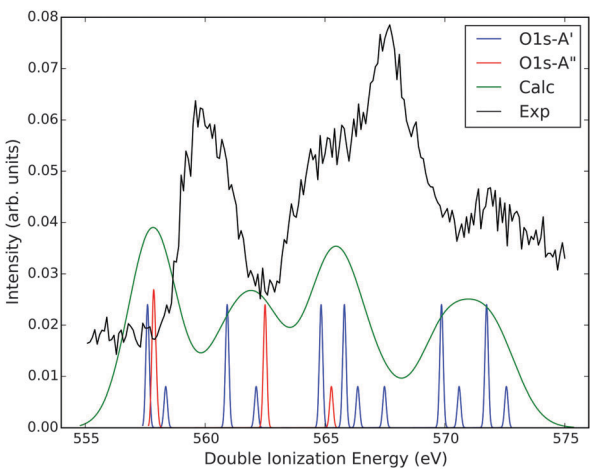

Fig. 12 MCSCF results of $O1s^{-1}v^{1}$.

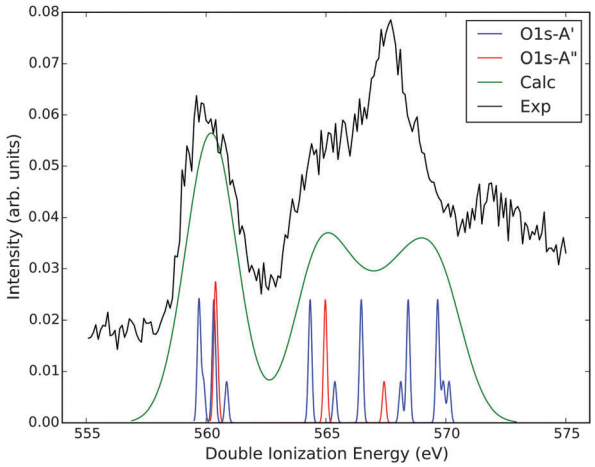

Fig. 13 SDCI results of $O1s^{-1}v^{1}$.

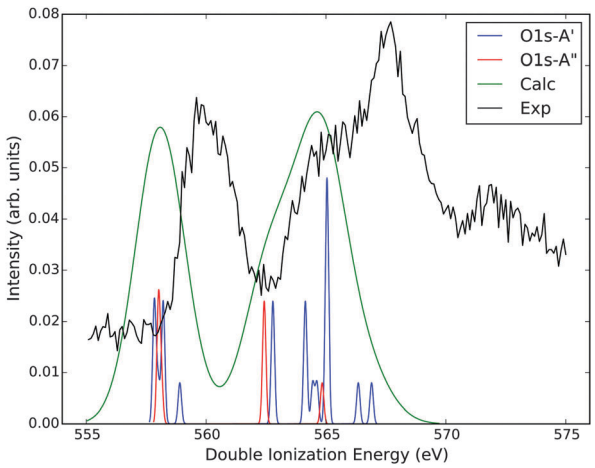

Fig. 14 CASPT2 results of $O1s^{-1}v^{1}$.

In the $Z + 1$ approximation the results listed in Table 4 have been calculated from the orbital energies and exchange integrals of Table 3. There are three sets of orbital energies in Table 3 which are calculated from the three different modified nuclear potentials (corresponding to each core hole state).

The Hartree–Fock calculations are carried out in several steps to avoid variational collapse. The core-hole state is calculated in two steps, first by freezing the core orbital and second, by relaxing the core while freezing the valence. The alternate freezing and relaxing of orbitals is itself an iterative procedure, but these two steps are generally sufficient to converge the energy. Next, for each individual valence orbital in the core-hole state an additional step is performed where one electron is removed, and both open-shells are frozen. We then use the converged high-spin triplet state orbitals to restart an open-shell singlet calculation, which generally converges in a few iterations. These steps give the triplet and singlet final energies at the Hartree–Fock level.

The MCSCF calculations are based on a complete active space wave function. In order to allow for ionisation of the 5–10σ and 1–2π electrons, we first promote these orbitals to the active space, leading to a ground state wave function with 4 inactive orbitals (the three core orbitals and a 4σ orbital). In the basic configuration we thus have 16 active electrons.

Table 2 Orbital energies and Coulomb and exchange integrals (atomic units) for selected molecular orbitals

c	ε_c	v	ε_v	J_{cv}	K_{cv}
O1s	−20.556	10σ	−0.427	0.783015	0.021657
		2π	−0.501	0.720922	0.016415
		9σ	−0.559	0.299559	0.003174
		1π	−0.606	0.298649	0.002689
		8σ	−0.623	0.675135	0.016998
		7σ	−0.674	0.620717	0.014739
		6σ	−0.805	0.427661	0.009638
		5σ	−1.023	0.289046	0.004264
$C_1$1s	−11.333	10σ	−0.427	0.444009	0.002154
		2π	−0.501	0.456039	0.003845
		9σ	−0.559	0.332420	0.001572
		1π	−0.606	0.359794	0.001989
		8σ	−0.623	0.513282	0.007869
		7σ	−0.674	0.502209	0.007871
		6σ	−0.805	0.552363	0.020443
		5σ	−1.023	0.452854	0.008810
$C_2$1s	−11.241	10σ	−0.427	0.331505	0.004071
		2π	−0.501	0.320231	0.002202
		9σ	−0.559	0.566490	0.009126
		1π	−0.606	0.559053	0.008504
		8σ	−0.623	0.403463	0.004677
		7σ	−0.674	0.369795	0.003390
		6σ	−0.805	0.375748	0.006366
		5σ	−1.023	0.664076	0.031461

Table 3 Orbital energies and exchange integrals (atomic units) for the $Z+1$ approximation

c	E[c] − E[gs]	v	ε_v	K_{cv}
O1s	19.763845	10σ	−0.800865	0.003548
		2π	−0.820217	0.014364
		9σ	−0.831541	0.003427
		8σ	−1.001978	0.006380
		1π	−1.031931	0.000335
		7σ	−1.095329	0.009881
		6σ	−1.183778	0.006747
		5σ	−1.324287	0.010301
$C_1$1s	10.826088	10σ	−0.788878	0.000812
		2π	−0.800088	0.000139
		9σ	−0.822355	0.002586
		8σ	−0.985881	0.011918
		1π	−0.927712	0.009069
		7σ	−1.053050	0.007569
		6σ	−1.193827	0.002596
		5σ	−1.398433	0.019315
$C_2$1s	10.720905	10σ	−0.699908	0.002776
		2π	−0.753349	0.031232
		9σ	−0.870001	0.076115
		8σ	−0.934505	0.084736
		1π	−0.984970	0.091203
		7σ	−1.000943	0.047278
		6σ	−1.107913	0.029683
		5σ	−1.524700	0.040107

The number of virtual orbitals in the Hartree–Fock picture to be included in the active space was guided by their MP2 natural occupation numbers. A choice of 3/2 additional active orbitals in symmetries A'/A'' leads to an active space of 9/4, *i.e.* 16 electrons in 13 orbitals. In the second step, the core-hole calculation, the wave function is reformatted to a restricted active space (RAS) wave function where the core-orbital is defined as singly occupied in RAS1, and the RAS2 space is identical to the CAS space in the ground state calculation. This allows us to optimize the core-hole state by the same alternate freezing and relaxing of core and remaining occupied orbitals as for Hartree–Fock. Finally, to treat all core–valence hole states on the same footing these relaxed core-hole orbitals where used for a configuration interaction calculation selecting 6 and 2 roots in symmetries A' and A'' respectively.

Table 4 Results of quantum chemical calculations of different core–valence states based on independent-particle models

	Koopmans		$Z+1$		Hartree–Fock	
Configuration	Triplet	Singlet	Triplet	Singlet	Triplet	Singlet
$O1s^{-1}$	559.355		—		537.802	
$C_1 1s^{-1}$	308.393		—		294.593	
$C_2 1s^{-1}$	305.878		—		291.733	
$O1s^{-1}10\sigma^{-1}$	591.698	592.877	559.498	559.691	558.253	558.734
$O1s^{-1}2\pi^{-1}$	592.144	593.038	559.730	560.512	558.779	558.803
$O1s^{-1}9\sigma^{-1}$	582.641	582.814	560.336	560.522	559.451	559.950
$O1s^{-1}8\sigma^{-1}$	583.885	584.032	564.893	565.240	564.214	565.083
$O1s^{-1}1\pi^{-1}$	594.218	595.143	565.873	565.891	562.967	565.033
$O1s^{-1}7\sigma^{-1}$	594.188	594.990	567.338	567.876	565.397	567.010
$O1s^{-1}6\sigma^{-1}$	592.633	593.158	569.830	570.197	567.992	569.608
$O1s^{-1}5\sigma^{-1}$	594.949	595.181	573.557	574.118	572.347	572.883
$C_1 1s^{-1}10\sigma^{-1}$	332.045	332.162	316.037	316.081	313.176	314.564
$C_1 1s^{-1}2\pi^{-1}$	334.320	334.529	316.361	316.368	315.108	315.146
$C_1 1s^{-1}9\sigma^{-1}$	332.620	332.706	316.900	317.041	315.583	315.612
$C_1 1s^{-1}8\sigma^{-1}$	334.609	334.717	321.096	321.744	320.438	321.055
$C_1 1s^{-1}1\pi^{-1}$	339.103	339.531	319.590	320.084	318.745	319.470
$C_1 1s^{-1}7\sigma^{-1}$	340.191	340.620	323.042	323.454	321.375	322.054
$C_1 1s^{-1}6\sigma^{-1}$	344.773	345.886	327.008	327.149	325.539	326.586
$C_1 1s^{-1}5\sigma^{-1}$	348.324	348.803	332.121	333.172	329.673	331.103
$C_2 1s^{-1}10\sigma^{-1}$	326.420	326.641	310.701	310.852	307.724	308.726
$C_2 1s^{-1}2\pi^{-1}$	328.157	328.277	311.380	313.080	310.047	310.060
$C_2 1s^{-1}9\sigma^{-1}$	336.272	336.769	313.333	317.476	313.428	313.544
$C_2 1s^{-1}8\sigma^{-1}$	337.343	337.805	314.854	319.466	316.313	316.834
$C_2 1s^{-1}1\pi^{-1}$	333.690	333.945	316.051	321.015	317.031	318.068
$C_2 1s^{-1}7\sigma^{-1}$	334.199	334.383	317.681	320.254	317.812	318.730
$C_2 1s^{-1}6\sigma^{-1}$	337.839	338.185	321.071	322.686	320.813	321.409
$C_2 1s^{-1}5\sigma^{-1}$	350.944	352.656	332.129	334.311	328.422	331.121

The SDCI calculations are based on allowing single- and double excitations out of the valence space into the virtual space. Here only the core orbitals are kept inactive (doubly occupied in the ground state or fixed single occupancy in the ionised states). We used a reduced RAS3 space in the expansion consisting of 29/16 active orbitals for symmetries A' and A'' respectively. In the ground state calculation we used the ground-state Hartree–Fock orbitals in the expansion and for the core–valence hole states we used the relaxed Hartree–Fock core-hole state orbitals in the expansion. The SDCI calculations have in most cases a dominant configuration (with CI-coefficients around 0.7–0.8). In Table 5 the ionisation energy at the SDCI level is accompanied by the leading configuration in the CI-expansion, which provides some insight into the nature of the excited ionised state. For the other correlated levels such a simple analysis is not possible as the optimized orbitals are arbitrary within a unitary transformation and can be mixed in any way as a result of the optimization.

Finally, for comparison we provide for a subset of the roots from CASPT2 calculations with Molcas,[29] which can be considered

Table 5 Results of different core–valence states based on correlated quantum chemical calculations. For each core hole and valence symmetry the roots are ordered by energy, and in the case of SDCI, the configuration with the leading coefficient is given in parenthesis

	CAS		SDCI		CASPT2	
Root	Triplet	Singlet	Triplet	Singlet	Triplet	Singlet
$O1s^{-1}$	537.813					
$C_1 1s^{-1}$	294.439					
$C_2 1s^{-1}$	290.804					
O–A'	557.600	558.358	559.704 (10σ)	559.890 (10σ)	557.842	558.004
	560.921	562.130	560.323 (9σ)	560.857 (9σ)	558.210	558.904
	564.836	566.367	564.339 (8σ)	565.370 (8σ)	562.785	564.446
	565.808	567.480	566.471 (7σ)	568.118 (7σ)	564.139	564.622
	569.859	570.593	568.429 (6σ)	569.892 (9σ[a])	565.041	566.347
	571.741	572.565	569.657 (9σ[a])	570.133 (6σ)	565.041	566.902
O–A''	557.844	557.951	560.381 (2π)	560.479 (2π)	558.016	558.135
	562.500	565.266	564.973 (1π)	567.423 (1π)	562.424	564.840
C_1–A'	312.337	312.243	313.812 (10σ)	313.839 (10σ)	313.519	313.460
	317.143	317.841	315.490 (9σ)	315.483 (9σ)	315.537	315.423
	317.274	318.677	319.137 (8σ)	319.906 (8σ)	317.143	317.930
	318.290	319.637	320.641 (7σ)	321.322 (7σ)	317.483	318.804
	319.311	320.743	321.695 (10σ[a])	322.670 (10σ[a])	318.654	320.157
	319.488	322.071	322.211 (10σ[a])	323.460 (10σ[a])	319.412	321.714
C_1–A''	314.399	314.201	315.189 (2π)	315.125 (2π)	314.945	314.821
	316.687	318.763	318.819 (1π)	319.820 (1π)	316.792	318.291
C_2–A'	308.196	308.484	308.883 (10σ)	309.142 (10σ)	308.566	309.188
	313.522	313.550	313.527 (9σ)	313.570 (9σ)	313.287	313.948
	315.798	316.305	315.427 (8σ)	315.959 (8σ)	315.317	316.084
	316.534	317.978	317.536 (7σ)	318.671 (7σ)	316.360	316.823
	318.124	319.312	319.732 (6σ)	320.415 (6σ)	316.639	319.332
	318.827	322.610	319.921 (10σ[a])	321.168 (10σ[a])	319.555	319.895
C_2–A''	311.277	311.286	311.580 (2π)	311.593 (2π)	311.773	311.773
	316.814	317.347	317.337 (1π)	318.524 (1π)	315.350	315.244

[a] The leading configuration is mixed with a $2\pi \rightarrow 3\pi$ excitation (shake-up).

the most sophisticated theoretical model in this set of calculations. The starting point for these calculations is the same active spaces as in our CAS calculations, the main difference thus being that an additional dynamic correlation is introduced with second-order perturbation theory. All other calculations have been made with the Dalton quantum chemistry program.[30]

All calculations were carried out with the cc-pVTZ basis set[31] and were performed at a fixed geometry obtained from ref. 32: the two carbon atoms and the oxygen atom of acetaldehyde form a backbone with bond lengths CO = 1.215 Å and CC = 1.494 Å, and form an angle of OCC = 124.1°. The formylic group, the central carbon and the oxygen, has a hydrogen attached to the carbon with bond length CH = 1.1094 Å, at an angle OCH = 119.7° with the CO-bond. The end carbon is the center of a methylic group: in the symmetry plane, a hydrogen is located at CH = 1.088 Å from the carbon and forms an angle HCO = 110.6° with the CO bond. The two symmetry equivalent methylic hydrogens have a bond length CH = 1.092 Å and form an angle of 110.0° with the CC axis. Finally, the two equivalent hydrogens form an angle HCH = 107.4°.

In Fig. 5–13 we display the results at the individual levels relative to the experimental spectra. The ionisation energies for each final state are displayed as a narrow Gaussians where the relative intensities between triplet and singlet states have a ratio of 3/1 but is otherwise arbitrary. The smooth profile represents the total computed spectrum obtained by a convolution using Gaussians of 0.7 eV width for the case of Fig. 5–14 and 1.4 eV for the case of Fig. 10–13. The color scheme in all these figures follow the same pattern. All roots in the A' symmetry are displayed as narrow blue peaks and all roots in the A'' symmetry by narrow red peaks. Singlet and triplet states are distinguished by different heights, the ratio 3/1 for triplet *versus* singlet states is a consequence of assigning all final states equal intensity, and can be seen when they are well separated. In the carbon 1s spectra, we distinguish between formylic and methylic contributions with different line style (solid *vs.* dashed). The total computed profile is given in green and the background experimental curve in black.

D. Carbon 1s

The computed spectra for carbon core–valence ionisation are shown in Fig. 5–9. In the numerical spectra there is one aspect in common for all levels of theory: the two peaks associated with the highest occupied molecular orbitals, 10σ and 2π and the methylic core hole, are clearly separated from the others, while the remaining peaks accumulate to a varying degree under

the broader feature of the experimental spectrum. It can be seen that the single-reference models have their highest root outside the recorded spectrum and far above the correlated values. A likely reason for this is because *e.g.* the highest root is forced to be the 5σ valence hole, which was not captured at the correlated levels – given the same number of roots there give raise to other structures of multi-configurational character at lower energies, which are not obtained with the simpler models.

In the $Z + 1$ approximation (*cf.* Fig. 5) the lowest peaks are close in energy and shifted by about 2 eV to the higher end of the spectrum. This approximation may qualitatively reproduce the lower end of the spectrum. As this simple model is based on a single-reference picture for the higher states as well, the singlet–triplet splitting is small throughout, which is not the case for the correlated calculations. The highest-energy peaks (corresponding to 5σ) are in this model by more than 10 eV outside the experimental spectrum.

The Hartree–Fock calculations produce a qualitatively correct structure for the lowest roots, but in contrast to the $Z + 1$ approximation the main features are shifted towards lower energy. It is possible to discriminate between the two lowest peaks belonging to the methylic carbon core hole, whereas the onset of the formylic carbon spectrum is mixed with the higher excitations of the methylic spectrum.

The MCSCF level represents a minimum level that qualitatively maps all calculated roots of the computed spectrum to the same energy range as the experimental spectrum. The lowest groups of roots are well separated from the others and can be identified with the methylic carbon and the 10σ and 2π hole states, at 309 and 311 eV respectively. The singlet–triplet splitting is very small and the peaks practically overlap. Peaks 3 and 4 at 314–315 eV can also be identified with the same valence orbitals for the formylic carbon hole state. Peaks 5 and 6 identified in the experimental spectrum are barely distinguished and form minor ripples in a broad spectral feature. The computations yield a close group of ionisation energies in the region of 316–324 eV.

The SDCI spectrum is qualitatively the same as for MCSCF, in particular for the lower peaks, while for the higher peaks the roots have a slightly different distribution. One visible difference is that the onset of the formylic spectrum is mixed with the higher roots of the methylic spectrum. Looking at the computational profile generated with broad Gaussian widths, the SDCI level has best overall resemblance with the experimental profile. In Table 5 we have included the leading configuration in the CI expansion. For the two highest roots associated with the formylic carbon we have combinations of ionisation of the 10σ electron and an excitation in the A'' symmetry ($2\pi \rightarrow 3\pi$). These two solutions are similar and differ only in the spin coupling order. Only the first four roots are dominated by single ionisations. For the methylic carbon the first five roots are dominated by single ionisations and the sixth root has a shake-up nature.

The CASPT2 results, displayed in Fig. 9, are similar to SDCI, but slightly shifted to lower energy. All levels allow us to interpret peaks 1 and 2 as methyl-HOMO and methyl-HOMO−1 (10σ and 2π) ionisations, while peak 3 marks the beginning of the formylic spectrum followed by a number of close-lying states representing a mixture of both carbon spectra.

E. Oxygen 1s

The computed spectra for Oxygen core–valence ionisations are presented in Fig. 10–13. The analysis is simpler for oxygen than carbon in acetaldehyde with only a single nucleus of this kind.

In the $Z + 1$ approximation for the oxygen core hole the results are not at all unreasonable. The lowest three roots corresponding to 10σ, 9σ and 2π including singlet and triplet combinations accumulate under the lowest main experimental peak, while the highest root 5σ is a about 1 eV higher than the highest-energy peak in the experimental spectrum. The inner valence roots overlap qualitatively with the mid experimental features (2–3).

In the Hartree–Fock picture, we obtain an overall shift of the computed spectrum towards lower energy, just as in the case of the carbon spectrum. At this level the lowest roots corresponding to 9–10σ and 2π match the lowest peak, while 5σ matches the highest peak and the remaining orbitals build up the intermediate broader feature.

At the MCSCF level the total spectrum appears shifted towards even lower energy but otherwise follows the experimental profile. The first large feature identified as experimental peak 1 corresponds to a close-lying group of energies involving the 10σ and 2π hole states. The singlet–triplet splitting is small here as well. For the higher roots the singlet–triplet separations are more pronounced. The highest experimental peak (3) coincides energetically with a mixture of roots involving 8σ and singlet 1π, whereas the highest computed root contains a mixture of ionisation in A' symmetry and excitation in A'' symmetry.

At the SDCI level (*cf.* Fig. 13) the computed profiles fit very well the experimental profile. The three lowest roots build up the first large peak, while the mid-part of the spectrum involves a mixture of 7–8σ and 2π orbitals. There is at this level of theory a slight energetic reordering – the highest root is indeed dominated by 6σ hole configurations and slightly below a shake-up structure involving the 9σ orbital, as well as a $2\pi \rightarrow 3\pi$ excitation.

At the CASPT2 level (*cf.* Fig. 14) the results for the lowest states are, as for the carbon case, very similar to the results obtained at the SDCI level. The three lowest states are characterized by the involvement of the 10σ, 9σ and 2π orbitals and are close in energy matching the first experimental peak. The next inner-valence holes contribute to the broad middle peak referred to as features 2–3 in the experimental spectrum.

V. Conclusions

Experimental core–valence double ionisation spectra of acetaldehyde (ethanal) were investigated at photon energies above the carbon and oxygen 1s ionisation edges using a versatile multi-electron coincidence spectroscopy technique. While the low energy part of the experimental spectra can tentatively be understood in terms of a simple shift model involving the known valence photoelectron spectrum, detailed understanding

of the core–valence spectra required quantum chemical calculations of increasing sophistication, leaning on the notion that modern electronic structure methods provide vast possibilities to analyse modern types of electron spectroscopies.

To begin with, the simpler computational models put forward, based on interaction corrected (Hartree–Fock) orbital energies or the $Z + 1$ approximation, were appealing because they gave reasonable results for the lower end of the spectrum in both the carbon and oxygen cases, and for the oxygen spectrum also the higher roots were not unreasonable. Furthermore, they gave simple orbital interpretations of the spectra and can straightforwardly be used also for ''large'' molecules. However, generally for the higher energy part of the spectrum, the real electronic structure is too complex for these simple models. From the case of acetaldehyde we see that electron correlation plays an important role, and that shake-up structures have to be accounted for which are intermixed with the simply ionised states.

There is no doubt that the CASPT2 method is the most sophisticated method of them all, but it is also the most expensive. The computed spectrum has the shape of the experimental spectrum but slightly shifted to a lower energy. The SDCI calculations that use HF orbitals for the ground state and core-relaxed orbitals for the core–valence ionised states, combine several important aspects that are important for modelling these states: the main part of the relaxation energy is accounted for as well as the correlation energy. In addition, it is the correlated level which most easily allows for an interpretation of the structure of the excited states, as in most cases the CI expansions are dominated by a single configuration.

All computational results presented in this study are based on energies of initial and final states. To simulate an experimental spectrum one needs in principle to calculate intensities as well, but this would introduce several additional difficulties that require proper treatment of continuum electrons and non-orthogonal basis sets, which are beyond the scope of this work. The simple assumption that all calculated roots are given equal intensity has been motivated by the experimental observation of the continuum electrons. With this assumption we have computed an ionisation profile broadened by Gaussian functions, which in the single and double excitation configuration interaction model has most consistently the best overall resemblance with the experimental spectrum. Thus this technique, based on single core hole optimised orbitals, seems to provide the best option to analyse core–valence double hole spectra considering precision and cost for molecules of the size studied here.

Acknowledgements

This work has been financially supported by the Swedish Research Council (VR) and the Knut and Alice Wallenberg Foundation, Sweden. We would like to warmly acknowledge the support by the staff and colleagues at the Helmholtz Centre for Materials and Energy GmbH BESSY-II, Berlin. This work was also supported by the European Community – Research Infrastructure Action under the FP6 ''Structuring the European Research Area'' Programme (through the Integrated Infrastructure Initiative ''Integrating Activity on Synchrotron and Free Electron Laser Science''. – Contract R II 3-CT-2004-506008). This work was supported by a grant from the Swedish Infrastructure Committee (SNIC) for the project ''Multiphysics Modeling of Molecular Materials'', SNIC 023/07-18.

References

1 J. H. D. Eland, O. Vieuxmaire, T. Kinugawa, P. Lablanquie, R. I. Hall and F. Penent, *Phys. Rev. Lett.*, 2003, **90**, 053003.
2 J. H. D. Eland, *Chem. Phys.*, 2003, **294**, 171.
3 J. H. D. Eland R. Feifel and D. Edvardsson, *J. Phys. Chem. A*, 2004, **108**, 9721.
4 R. Feifel, J. H. D. Eland and D. Edvardsson, *J. Chem. Phys.*, 2005, **122**, 144308.
5 R. Feifel, J. Eland, L. Storchi and F. Tarantelli, *J. Chem. Phys.*, 2005, **122**, 144309.
6 P. Linusson, L. Storchi, F. Heijkenskjöld, E. Andersson, M. Elshakre, B. Pfeifer, M. Colombet, J. H. D. Eland, L. Karlsson, J.-E. Rubensson, F. Tarantelli and R. Feifel, *J. Chem. Phys.*, 2008, **129**, 234303.
7 Y. Hikosaka, T. Aoto, P. Lablanquie, F. Penent, E. Shigemasa and K. Ito, *Phys. Rev. Lett.*, 2006, **97**, 053003.
8 E. Andersson, P. Linusson, S. Fritzsche, L. Hedin, J. H. D. Eland, L. Karlsson, J.-E. Rubensson and R. Feifel, *Phys. Rev. A: At., Mol., Opt. Phys.*, 2012, **85**, 032502.
9 Y. Hikosaka, T. Kaneyasu, E. Shigemasa, P. Lablanquie, F. Penent and K. Ito, *J. Chem. Phys.*, 2007, **127**, 044305.
10 E. Andersson, M. Stenrup, J. H. D. Eland, L. Hedin, M. Berglund, L. Karlsson, A. Larson, H. Ågren, J.-E. Rubensson and R. Feifel, *Phys. Rev. A: At., Mol., Opt. Phys.*, 2008, **78**, 023409.
11 E. Andersson, J. Niskanen, L. Hedin, J. H. D. Eland, P. Linusson, L. Karlsson, J.-E. Rubensson, V. Carravetta, H. Ågren and R. Feifel, *J. Chem. Phys.*, 2010, **133**, 094305.
12 J. Niskanen, V. Carravetta, O. Vahtras, H. Ågren, H. Aksela, E. Andersson, L. Hedin, P. Linusson, J. H. D. Eland, L. Karlsson, J.-E. Rubensson and R. Feifel, *Phys. Rev. A: At., Mol., Opt. Phys.*, 2010, **82**, 043436.
13 J. Niskanen, E. Andersson, J. H. D. Eland, P. Linusson, L. Hedin, L. Karlsson, R. Feifel and O. Vahtras, *Phys. Rev. A: At., Mol., Opt. Phys.*, 2012, **85**, 023408.
14 H. Ågren, A. Cesar and C. Liegener, *Adv. Quantum Chem.*, 1992, **23**, 1.
15 D. Chadwick and A. Katrib, *J. Electron Spectrosc. Relat. Phenom.*, 1974, **3**, 39.
16 W.-C. Tam, D. Yee and C. Brion, *J. Electron Spectrosc. Relat. Phenom.*, 1974, **4**, 77.
17 K. Kimura, S. Katsumata, T. Yamazaki and H. Wakabayashi, *J. Electron Spectrosc. Relat. Phenom.*, 1975, **6**, 41.
18 R. Bombach, J.-P. Stadelmann and J. Vogt, *Chem. Phys.*, 1981, **60**, 293.
19 K. Johnson, I. Powis and C. Danby, *Chem. Phys.*, 1982, **70**, 329.

20 M. Keane, S. Lunell, A. de Brito, M. Carlsson-Göthe, S. Svensson, B. Wannberg and L. Karlsson, *J. Electron Spectrosc. Relat. Phenom.*, 1991, **56**, 313.
21 N. Correia, A. Naves de Brito, M. P. Keane, L. Karlsson, S. Svensson, C.-M. Liegener, A. Cesar and H. Ågren, *J. Chem. Phys.*, 1991, **95**, 5187.
22 D. Minelli, F. Tarantelli, A. Sgamellotti and L. Cederbaum, *J. Electron Spectrosc. Relat. Phenom.*, 1995, **74**, 1.
23 S. Zagorodskikh, V. Zhaunerchyk, M. Mucke, J. H. D. Eland, R. J. Squibb, P. Linusson and R. Feifel, *Chem. Phys.*, 2015, **463**, 159.
24 P. Kruit and F. H. Read, *J. Phys. E: Sci. Instrum.*, 1983, **16**, 313.
25 S. Plogmaker, P. Linusson, J. H. D. Eland, N. Baker, E. M. J. Johansson, H. Rensmo, R. Feifel and H. Siegbahn, *Rev. Sci. Instrum.*, 2012, **83**, 013115.
26 G. C. King, M. Tronc, F. H. Read and R. C. Bradford, *J. Phys. B: At. Mol. Phys.*, 1977, **10**, 2479.
27 C. Møller and M. S. Plesset, *Phys. Rev.*, 1934, **46**, 618.
28 C. David Sherrill and H. F. Schaefer III., *Adv. Quantum Chem.*, 1999, **34**, 143–269.
29 F. Aquilante, L. De Vico, N. Ferré, G. Ghigo, P.-Å. Malmqvist, P. Neogrády, T. B. Pedersen, M. Pitonak, M. Reiher, B. O. Roos, L. Serrano-Andrés, M. Urban, V. Veryazov and R. Lindh, *J. Comput. Chem.*, 2010, **31**, 224.
30 K. Aidas, C. Angeli, K. L. Bak, V. Bakken, R. Bast, L. Boman, O. Christiansen, R. Cimiraglia, S. Coriani, P. Dahle, E. K. Dalskov, U. Ekström, T. Enevoldsen, J. J. Eriksen, P. Ettenhuber, B. Fernández, L. Ferrighi, H. Fliegl, L. Frediani, K. Hald, A. Halkier, C. Hättig, H. Heiberg, T. Helgaker, A. C. Hennum, H. Hettema, E. Hjertenæs, S. Høst, I.-M. Høyvik, M. F. Iozzi, B. Jansik, H. J. Aa. Jensen, D. Jonsson, P. Jørgensen, J. Kauczor, S. Kirpekar, T. Kjærgaard, W. Klopper, S. Knecht, R. Kobayashi, H. Koch, J. Kongsted, A. Krapp, K. Kristensen, A. Ligabue, O. B. Lutnæs, J. I. Melo, K. V. Mikkelsen, R. H. Myhre, C. Neiss, C. B. Nielsen, P. Norman, J. Olsen, J. M. H. Olsen, A. Osted, M. J. Packer, F. Pawlowski, T. B. Pedersen, P. F. Provasi, S. Reine, Z. Rinkevicius, T. A. Ruden, K. Ruud, V. Rybkin, P. Salek, C. C. M. Samson, A. Sánchez de Merás, T. Saue, S. P. A. Sauer, B. Schimmelpfennig, K. Sneskov, A. H. Steindal, K. O. Sylvester-Hvid, P. R. Taylor, A. M. Teale, E. I. Tellgren, D. P. Tew, A. J. Thorvaldsen, L. Thøgersen, O. Vahtras, M. A. Watson, D. J. D. Wilson, M. Ziolkowski and H. Ågren, *WIREs Comput. Mol. Sci.*, 2014, **4**, 269.
31 T. H. Dunning Jr., *Chem. Phys.*, 1989, **90**, 1007–1023.
32 T. Nakano, K. Morihashi and O. Kikich, *Ab initio* study of Σ and Π electronic states of formyl reactions, *THEOCHEM*, 1992, **253**, 161–166.